Ground motion studies of modern and historical Cascadia intraslab earthquakes using one and three dimensional waveform modeling methods to generate ground shaking maps

04HQGR0050

Gene A. Ichinose
URS Group, Inc.
566 El Dorado Street, 2nd Floor
Pasadena, CA 91101-2560
Phone 626-449-7650, Fax 626-449-3536, email gene_ichinose@urscorp.com
Key Words: Source characteristics, strong ground motion, loss estimation,

Investigations undertaken

1. Analysis of moment tensors of recent Puget Sound intraslab earthquakes
2. Rupture process of the 1949 Olympia earthquake
3. Source scaling relationships for intraslab earthquakes

Results

1. *Analysis of moment tensors of recent Puget Sound intraslab earthquakes*

We inverted long-period regional-waves for the point-source moment tensors of 4 intraslab earthquakes (Table 1; Fig. 1) using the methodology similar to *Ritsema and Lay* [1995]. Long-period waves are insensitive to the complexities from source-finiteness and path propagation effects given that the dominant period of the waves is larger than the dimensions of the source and earth heterogeneities. The reflectivity and frequency and wave-number summation technique [*Zeng and Anderson*, 1995] is used to compute the Green's functions. We use the WUS velocity model constructed from phase velocity measurements of surface waves across the tectonically active regions of the western U.S. [*e.g.*, *Ritsema and Lay*, 1995]. The receivers are distributed across different tectonic regions and therefore the choice of the velocity model depends more on the site and path than on source structure.

Table 1. Regional-wave Moment Tensor Inversion Results

Date	Origin Time	Nodal Plane 1 Strike/Dip/Rake	Nodal Plane 2 Strike/Dip/Rake	Mo (dyne×cm)	M_w	Depth (km)	PDC(1)	Location
1999/07/03	01:43:55	206°/45°/-44°	330°/60°/-126°	4.81×10^{24}	5.72	40	98%	Satsop
2001/02/28	18:54:33	196°/22°/-67°	351°/68°/-98°	1.11×10^{26}	6.67	60	89%	Nisqually
2001/06/10	13:19:09	136°/34°/-106°	337°/58°/-80°	1.36×10^{23}	4.69	40	98%	Satsop
2003/04/25	10:02:13	252°/9°/-56°	38°/82°/-95°	6.76×10^{22}	4.49	46	79%	Mt Olympus

(1) Percent Double Couple

U.S. National Seismic Network, Global Seismic Network (IRIS), and Canadian Digital Seismic Network broadband seismograms are instrument corrected to displacement and filtered between 200-20 sec for the M 6.8 earthquake and 100-10 sec for the smaller M < 5 earthquakes. We use the Pacific Northwest Seismic Network (University of Washington) epicenter locations to compute a suite of Green's functions for 2 km depth increments and shift the data by increments of 1 sec in origin-time. We then iteratively solve for the centroid depth and origin time using a grid search to search for minima of the L2-norm objective function while maximizing the percent double-couple. We solve for the deviatoric moment tensor assuming no volume change. With a wide range of wave frequencies and station distances, the inversions become heavily weighted toward higher frequencies and larger amplitudes from near-field stations. We do not apply distance weighting, although there is a natural weighting with distance because the farther stations usually have more data points. These inversions are also weighted more toward the surface than body waves because of the difference in amplitudes. The depths of these 4 earthquakes are ~5-10 km below the top of the subducting Juan de Fuca plate indicating that they are within the slab-crust resulting from localized tensile stresses within the plate. The stresses may be related to mineral phase transitions in the slab-crust from epidote-amphibolite to eclogite through a process of

dehydration [*Hacker et al.*, 2002; *Dobson et al.*, 2003]. An alternative or contributing cause to the stresses may be related to a bend in the slab where the largest earthquakes have previously occurred in the Puget Sound and Strait of Georgia.

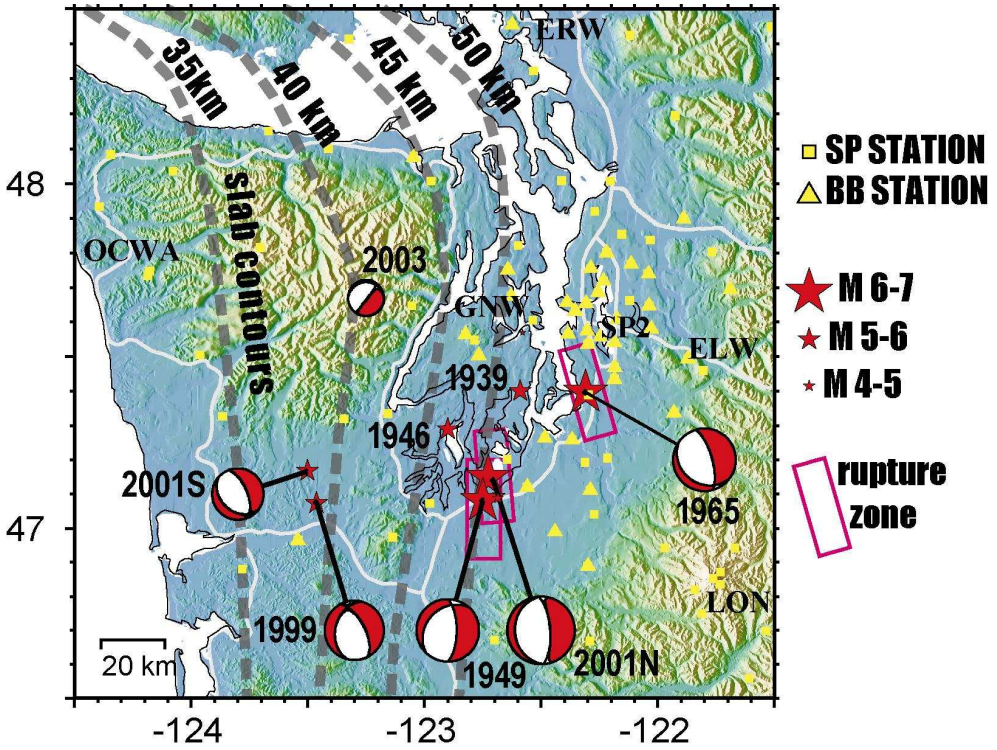

Figure 1. Locations and mechanisms of Puget Sound intraslab earthquakes. The mechanisms were determined from point source moment tensor inversions. There were 2 earthquakes in 2001, near Satsop (2001S) and Nisqually (2001N). The contours show the approximate depth to the top of the subducting Juan de Fuca plate.

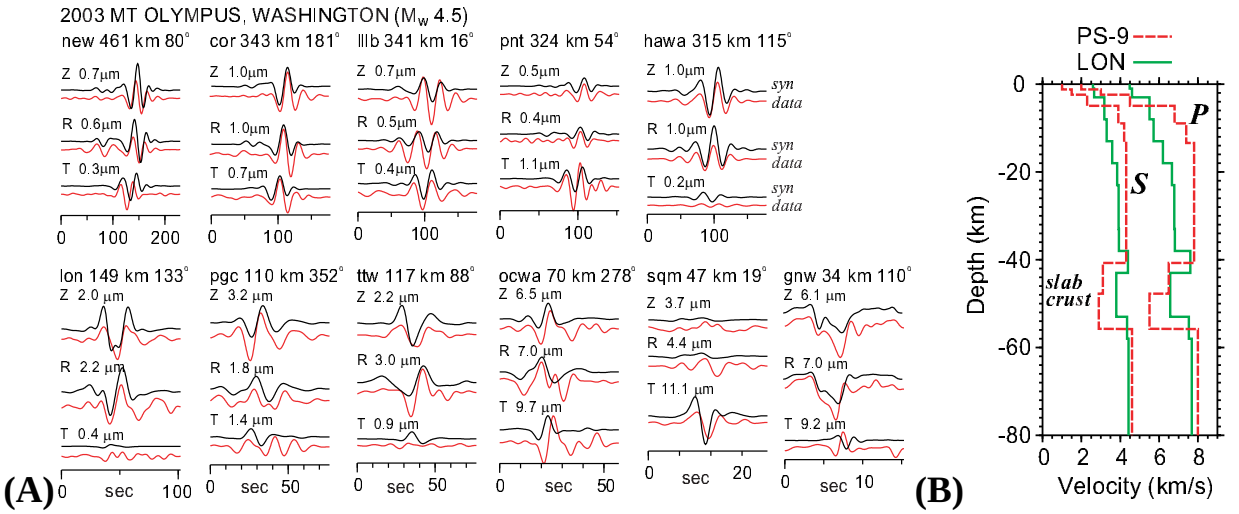

Figure 2. (A) Observed and predicted displacements for the 2003 Mt. Olympus (M_w 4.5) earthquake estimated from the moment tensor inversion. The station distance in km and azimuth in degrees from north are labeled above the waveforms. The amplitudes are in units of microns. (B) The PS-9 velocity model [*Langston and Blum*, 1977] is compared to the LON model [*Ichinose et al.*, 2003a, 2004], which was used in the computation of Green's functions for the moment tensor and finite-fault slip inversions.

2. Rupture process of the 1949 Olympia, Washington earthquake

Cascadia intraslab earthquakes have occurred frequently in the Puget Sound including in 1949 (M 7), 1965 (M 6.9), 1999 (M_w 5.9) and 2001 (M_w 6.8). The hazard they pose is equal to other seismic sources for time scales relevant to retrofitting (50% probability of exceedance in 75 yrs). Reexamination of historical earthquake records and analysis of digital broadband seismograms from recent earthquakes improves strong motion prediction more than stochastic scenarios and better resolves how stresses are released in the subducting slab relative to stresses from external tectonic forces and local dehydration. Reanalysis of the 1949 Olympia earthquake using digitized seismograms collected by *Barker and Langston* [1987], *Wiest et al.* [2004], and long-period WWSSN data from College, AK, Bogotá, Columbia, and Pasadena, CA, yielded a normal-slip mechanism with ~E-W extensional-axis. This mechanism resembles those from previous Puget Sound intraslab earthquakes (Figure 1). The strike-slip mechanism estimated by *Baker and Langston* [1987] contrasted greatly because past Puget Sound intraslab earthquakes all have normal-slip mechanisms although strike-slip and thrust mechanisms for intraslab earthquakes have occurred in other subduction zones (*e.g*, Nankai Trough).

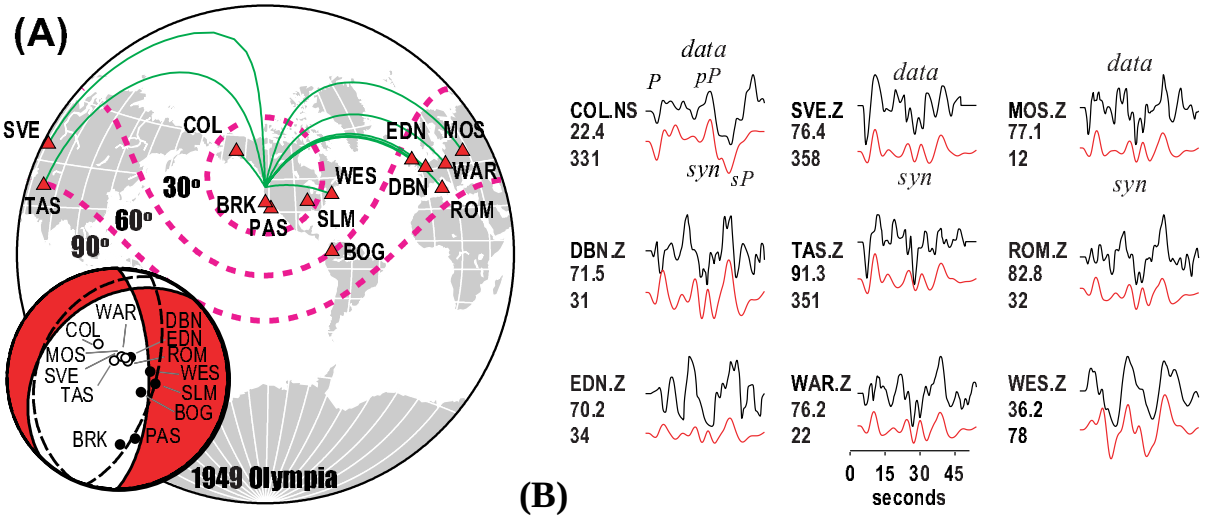

Figure 3. **(A)** Teleseismic stations that recorded the 1949 Olympia, Washington earthquake. The shaded mechanism shows the overall moment release while the nodal planes with dashed lines are from the first subevent. First motion polarities from Berkeley (BRK), Bogotá (BOG), Pasadena (PAS), Saint Louis (SLM), and Weston (WES) constrain the dip of the high angle plane for the first subevent. The first motion polarities are more consistent with that predicted by the initial subevent, including BOG not used by *Baker and Langston* [1987]. **(B)** Observed and predicted teleseismic P-waves from 9 stations used in the inversion. Epicenter distance in (°) and source-receiver azimuth are listed below the station code.

We used a time-domain iterative inversion method of *Kikuchi and Kanamori* [1991] that inverts teleseismic body waves to determine the mechanisms and rupture process of large earthquakes. The rupture process is represented as a sequence of subevents distributed in space and time each with a finite duration. The individual subevent mechanisms and sizes are allowed to vary during the sequence. The number unknowns are limited from observational constraints and a grid search is performed over the other free parameters including hypocenter depth, rupture direction, subevent rise time and rupture velocity to find the waveform fit with the lowest L2-norm error. Figure (3A) shows the distribution of teleseismic stations which yielded P-waveform or first motion polarity data. We apply the instrument corrections to the Green's functions to avoid instabilities due to the instrument deconvolution to digitized data. We initially used the PS-9 velocity model [*Langston and Blum*, 1977] but found that our calibrated LON velocity model [*Ichinose et al.*, 2003a; 2004] produced lower errors and better waveform fits (Figure 2B). Figure (3B) shows the observed and predicted vertical and north-south component P-waves. We assume 2 subevents with the second occurring some time between 0 and 5 sec. The grid search shows

that a rise time of 3 sec best fits the frequency character of the waveform data while there is no resolution of rupture velocity with this global teleseismic station distribution. We therefore chose a velocity of 3.5 km/s that was close to V_r = 0.8 V_s where V_s = 4.38 km/s between 50-60 km depth. Figure 4 shows the earthquake ruptured southward along a plane with 170/350° strike and 70°E dip. The hypocenter depth is at 60 km and the total M_o is 1.9×10^{26} dyne-cm (M_w 6.7). The amplitudes from the vertical component Pasadena 1-90 sec Benioff record indicate a similar M_w ~ 6.8 when compared to those from the 2001 Nisqually earthquake convolved with a similar response (Figure 5).

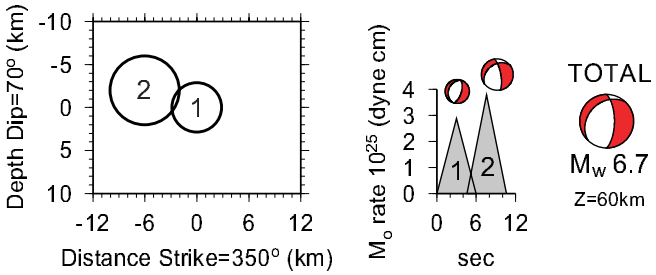

Figure 4. The 1949 Olympia earthquake subevent locations and mechanisms and source time functions (Table 2).

Table 2. 1949 Olympia, Washington earthquake source parameters

Subevent	Nodal Plane 1 Strike/Dip/Rake	Nodal Plane 2 Strike/Dip/Rake	Depth (km)	M_o (dyne-cm)	T_0 (s)	T_r (s)
1	204/28/-83°	16/62/-93°	60	0.58×10^{26}	0	3
2	233/36/-31°	349/72/-122°	58	0.76×10^{26}	4.6	3
sum	223/31/-51°	0/66/-111°	60	1.28×10^{26}	0	-

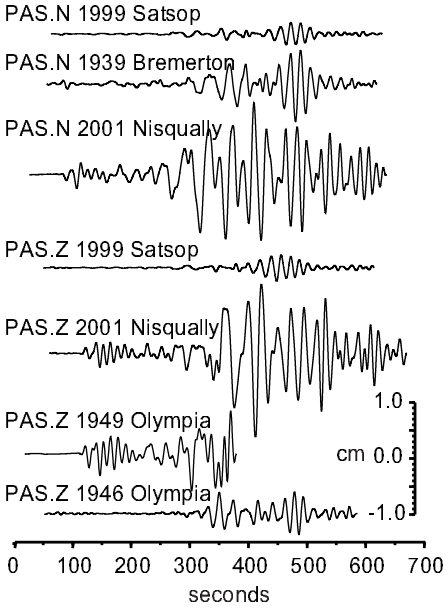

Figure 5. Digitized seismograms from the historical 1946 Olympia, 1939 Bremerton, and 1949 Olympia earthquakes compared to modern digital records of the 1999 Satsop (M_w 5.8) and 2001 Nisqually (M_w 6.8) earthquakes filtered and scaled to the same frequency bands and amplitude gains of the Pasadena (PAS) 1-90 Benioff instrument. Based on the similarity between waveforms, the 1949 Olympia earthquake may have been similar in size or slightly larger than the 2001 Nisqually earthquake. The 1946 Olympia (or Satsop?) event appears to be an order of magnitude smaller than the 2001 Nisqually earthquake.

The southward rupture propagation is hard to confirm since there are no stations to the south except for PAS whose P-wave ray path is bottoming in the transition zone and may also be complicated by the triplicated P-wave phases from upper-mantle 410 km discontinuity. A more rigorous method is needed to model the PAS waveforms.

We inverted the 9 teleseismic P-waves for the spatial and temporal distribution of slip and rake. Our method is explained by *Thio et al* [2004] and is similar to the multiple time window method of *Hartzell and Heaton* [1983]. The fault plane is described by a grid of points for which Green's functions are

computed at each grid to observation point. A propagating slip band is imposed from the hypocenter and propagates at a fixed number of time steps. This slip band is characterized by 2 parameters, maximum rupture velocity and rise time. Grid points that are contained within a slip band, at each time step, are combined and cast into a set of normal equations. The normal equation is solved simultaneously using a least squares solver with a positivity constraint to disallow reverse slip [*Lawson and Hanson*, 1974]. Regularization and spatial smoothing are applied to prevent wildly oscillating solutions. This is achieved by imposing a smoothing condition in which the amplitude of slip at one point is forced to be equal to its neighbors leading to models from varying complexity to models with uniform slip. *Thio et al* [2004] allows for variable rake, in which case every initial rake vector is split into 2 conjugate vectors where the new rake is different from the initial by ±45° so that the same positivity constraint can be used. The final rake vector is the vector summation of the two individual rake vectors. Allowing for variable rake thus leads to a doubling of the number of unknowns, so we regularized the 2 slip vectors to prevent strong, unphysical variation in rake. This is achieved in a manner analogous to the spatial smoothing, where instead of forcing the amplitude of a slip vector to be equal to its neighbors; we force it to be equal to its conjugate slip vector. A strong smoothing constraint causes the 2 conjugate vectors to become equal yielding the orientation of the initial rake vector. We imposed a weighting scheme that uses overall weight per data type, and within each group, an automatic weighting based on the absolute amplitude and number of points (*e.g., Thio et al.* [2004] and *Ichinose et al.* [2003b]). This was made to prevent the contribution of one dataset from dominating the solution especially in the case of greatly varying amplitudes and sample lengths. Inversion weighting parameters including those for slip and rake smoothing were selected on the basis of trial and error.

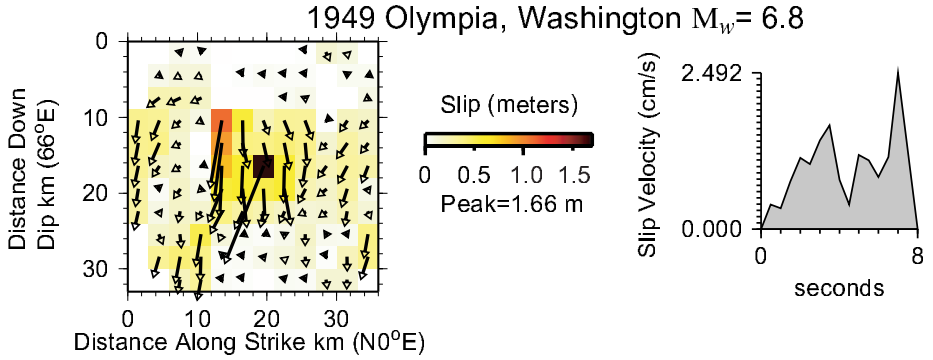

Figure 6. The 1949 Olympia earthquake cumulative slip and rake distribution estimated from the inversion of teleseismic data. The rake vectors point in the direction of the hanging wall motion. The hypocenter at 60 km is located at 16 km down dip and 20 km along strike. The distribution of slip, overall rake, and slip velocity results are very similar to the results obtained from a similar inversion for the mechanism and simple slip distribution shown in Figure 4.

The fault plane is parameterized as a rectangular grid of points 36 km along strike and 33 km down dip oriented in a N11°E direction dipping 66°E (Figures 4 and 6). This orientation was obtained from the same teleseismic P-waves and polarities. The fault plane is a grid of 12 by 11 points using a node/grid spacing of 3×3 km. We do not use subfaults or finer grid spacing so there are no subfault dynamics. A single Green's function computed for each grid point is adequate [*e.g., Beresnev and Atkinson*, 2001] given the poor quality and quantity of data. The hypocenter was placed in the middle of the fault given a location listed in the ISC earthquake catalog. We allow the rupture to evolve temporally based on a maximum rupture velocity of 3 km/s, a minimum rise time of 0.5 s, and a maximum rise time of 1 s. The 14 time windows are spaced 0.5 s apart. Any point on the fault can slip either 1 or 2 times after the passage of the rupture front. We expect rise times of about 1/10th of the total 8-10 sec duration of rupture, which is about 1 s, while an alternative estimate using a relation of *Somerville et al.* [1999] suggests a rise time of 1.1 s. The slip at each grid point is summed using an isosceles triangle shaped source-time function with 0.5 s rise and 0.5 s fall-off. Half the duration of this source-time function

controls the minimum rise-time. The total seismic moment (M_o) of 1.9×10^{26} dyne-cm (M_w 6.78) and slip distribution shown in Figure (6) is similar to the simple rupture process and total moment determined using the same data shown in Figure 4. The source parameters for this slip model are listed in Table 3.

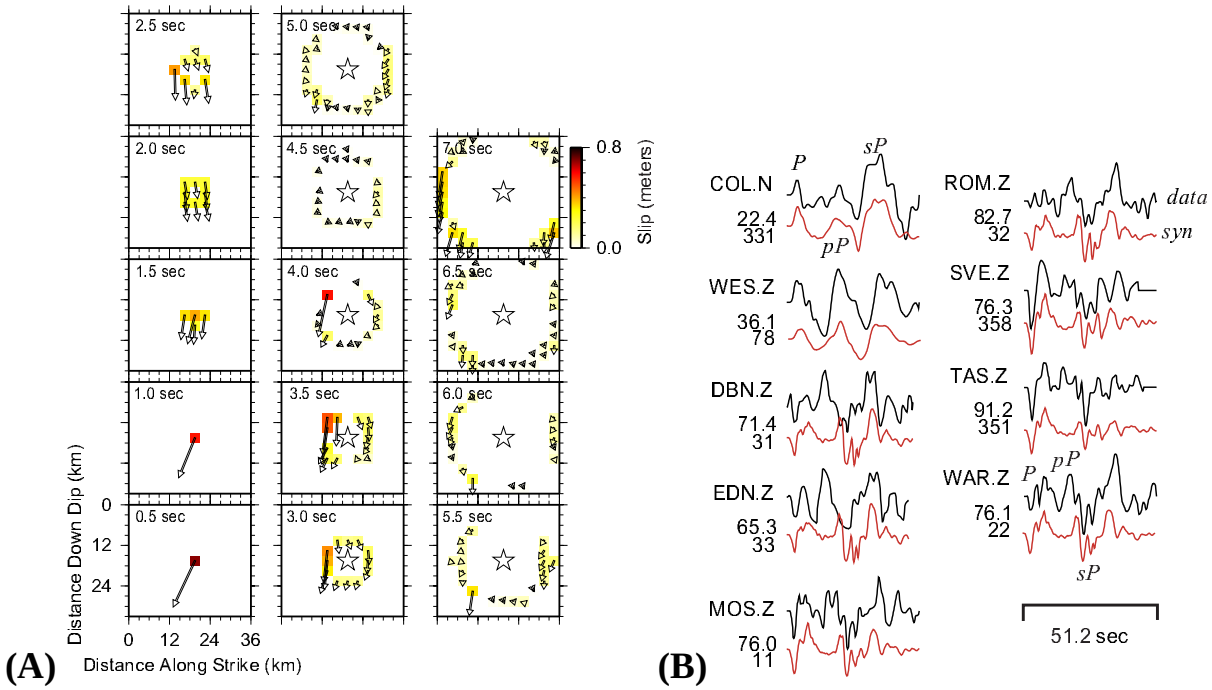

Figure 7. (A) Time progression of slip in 0.5 sec increments. Rake vectors indicate hanging wall motion. Star denotes the hypocenter at 60 km depth. **(B)** Observed and predicted teleseismic P-waves and depth phases computed from the slip model shown in Figure (7A).

3. Source scaling relationships for intraslab earthquakes

The rupture model of the 1949 earthquake has important implications for earthquake source scaling relations used for the simulation of strong-ground motions [e.g., *Somerville et al*., 1999]. One of these is the relationship between the seismic moment of the earthquake and the fault rupture area. This relationship is important because it defines the static stress drop, which affects the rate of energy release of the earthquake. It is commonly thought that intraslab earthquakes have smaller rupture areas or larger slip and hence larger static stress drops (and thus potentially stronger ground motions) than crustal or subduction zone-thrust earthquakes of the same size.

Figure 8 compares the source parameters from the 1949 Olympia earthquake (Table 3) with those obtained using similar procedures and methods for other Puget Sound and Japanese intraslab earthquakes [*Asano et al.*, 2003] and global crustal earthquakes [*Somerville et al*., 1999]. The rupture areas listed in Table 3 were calculated from the inversion results in this study or using similar inversion methods. The rupture area is the sum of the fault elements with slip greater than 0 multiplied by the element area. The comparisons include the scaling relationships between scalar seismic moments and rupture area, average slip, and characteristics of the asperities derived by *Somerville et al.* [1999] using global crustal earthquakes with the assumption of self-similarity. The M_o versus rupture area, average slip and asperity slip (Table 3) plot within the scatter of measurements from estimated slip models of global crustal earthquakes [*Somerville et al*., 1999]. The exception is with M_o versus asperity area, which indicates that intraslab earthquakes may have higher asperity stress drops possibly consistent with results from Japanese intraslab earthquakes. A global definition for asperity area is needed to better resolve this issue.

Future Work

1. Spectral Analysis and estimation of source parameters of intraslab earthquakes. We are planning to model S-wave coda envelopes to estimate the frequency (f) dependent intrinsic and scattering attenuation required to determine the static stress drop of the smaller 1999 and 2001 Satsop and 2003 Mount Olympus earthquakes. The spectra are modeled using a simple f^{-2} spectral shape with a single corner f_c and a Q(f) correction. These results will greatly add to the source scaling database for Puget Sound intraslab earthquakes and help resolve the apparent difference in scaling relation for asperity area and moment.
2. Ground shaking maps from the modern and historical intraslab earthquakes for rock sites. With the slip models of the 1949, 1965, and 2001 Nisqually earthquakes, we will compute ground shaking maps of PGA, PGV, SA at T = 0.3, 1, and 3 sec using a 1D hard rock velocity model.

Table 3. Summary of source parameters of 3 major PS intraslab earthquakes

	1949 Olympia	1965 Seattle-Tacoma	2001 Nisqually
M_o (dyne-cm)	1.91×10^{26}	9.43×10^{25}	1.66×10^{26}
Rupture Area	1026 km^2	248 km^2	496 km^2
Average Slip	0.22 m	0.52 m	0.43 m
Asperity Area[1] (combined)	18 km^2	28 km^2	45 km^2
Asperity Slip[1] (average)	1.37 m	2.15 m	1.67 m

[1]Nodes with slip > 1 m are defined as asperities.

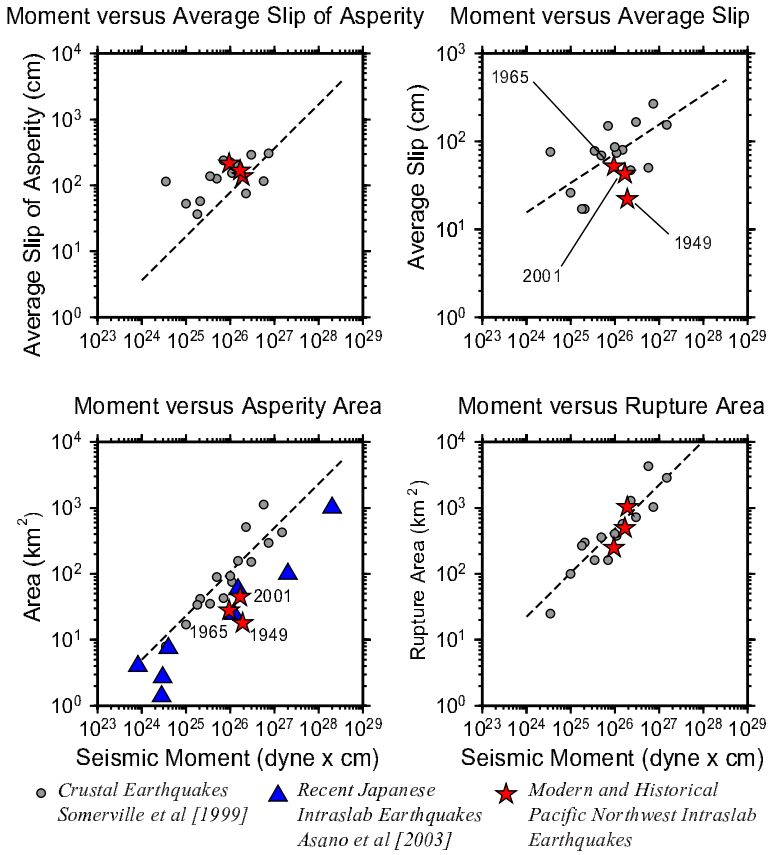

Figure 8. Relation between seismic moment and average slip, rupture area, asperity area, and average slip of asperity (Table 2) for the Puget Sound intraslab earthquakes "*stars*", Japanese intraslab earthquakes "*triangles*", and global crustal earthquakes "*circles*". *Somerville et al.* [1999] estimated the source scaling relations (dashed line) using a least square fit to source parameters of a set of crustal earthquakes assuming self-similarity.

References

Asano, K., T. Iwata, and K. Irikura, Source characteristics of shallow intraslab earthquakes derived from strong motion simulations, Earth Planets Space, 55, e5-e8, 2003.

Baker, G. E., and C. A. Langston, Source parameters of the 1949 magnitude 7.1 south Puget Sound, Washington, earthquake as determined from long-period body waves and strong motions, Bull. Seismol. Soc. Am., 77, 1530-1557, 1987.

Beresnev, I, and G. Atkinson, Subevent structure of large earthquakes - A ground motion perspective, Geophys. Res. Lett., 28, 53-56, 2001.

Dobson, D. P., P. G. Meredith, S. A. Boon, Simulation of subduction zone seismicity by dehydration of serpentine, Science, 298, 1407-1410, 2002.
Hacker, B. R., G. A. Abers, and S. M. Peacock, Theoretical mineralogy, density seismic wave speeds, and H2O content of the Cascadia subduction zone, with implications for intermediate-depth seismicity and earthquake hazard, in Intraslab Earthquakes in the Cascadia Subduction System: Science and Hazard, U.S. Geological Survey Circular, in press., 2003.
Hartzell, S. H., and T. H. Heaton, Inversion of strong motion and teleseismic waveform data for the fault rupture history of the 1979 Imperial Valley, California earthquake, Bull. Seism. Soc. Am., 73, 1553-1583, 1983.
Ichinose, G. A., Thio, Hong Kie, and P. G. Somerville, Source characteristics of modern and historical in-slab Cascadia earthquakes applicable to strong ground motion prediction, U. S. Geological Survey, NEHRP Final Technical Report, Award #02HQGR0018, 2003a.
Ichinose, G. A., Hong Kie Thio, and P. G. Somerville, Rupture process of the 1944 Tonankai earthquake (Ms 8.1) from the inversion of teleseismic and regional seismograms, J. Geophys. Res., 108(B10), 2497, doi: 10.1029/2003JB002393, 2003b.
Ichinose, G. A., H. K. Thio, P. G. Somerville, Rupture process and near source shaking of the 1965 Seattle-Tacoma and 2001 Nisqually intraslab earthquakes, Geophys. Res. Lett., 31, L10604, doi: 10.1029/ GL019668, 2004.
Kikuchi, M., and H. Kanamori, Inversion of complex body waves-III, Bull. Seism. Soc. Am., 81, 2335-2350, 1991.
Langston, C. A., and D. E. Blum, The April 29, 1965, Puget Sound earthquake and the crustal and upper mantle structure of western Washington, Bull. Seism. Soc. Am., 67, 693-711, 1977.
Lawson, C. L., and R. J. Hanson, Solving Least Squares Problems, Englewood Cliffs, NJ: Prentice-Hall, 1974.
Ritsema, J., and T. Lay, Long period regional wave moment tensor inversion for earthquakes in the western United States, J. Geophys. Res., 100, 9853-9864, 1995.
Somerville, P., K. Irikura, R. Graves, S. Sawada, D. Wald, N. Abrahamson, Y. Iwasaki, T. Kagawa, N. Smith, and A. Kowada, Characterizing crustal earthquake slip models for the prediction of strong ground motion, Seismol. Res. Lett., 70, 59-80, 1999.
Thio, H. K., R. W. Graves, P. G. Somerville, T. Sato, and T. Ishii, The source process of the 1999 Kocaeli (Turkey) Earthquake, J. Geophys. Res., (submitted), 2004.
Wiest, K., D. I. Doser, and J. Zollweg, Source processes of Western Washington intraslab earthquakes (1939-1965), (abstract), Seismol. Res. Lett., 74, 239, 2003.
Zeng, Y., and J. G. Anderson, A method for direct computation of the differential seismogram with respect to the velocity change in a layered elastic solid, Bull. Seismol. Soc. Am., 85, 300-307, 1995.

Non-Technical Summary

Intraslab earthquakes occur inside the subducting Juan de Fuca plate deep (> 40 km) beneath the Puget Sound (PS) of western Washington state and have occurred frequently including in 1949 (M_w 6.8), 1965 (M_w 6.8), 1999 (M_w 5.9) and 2001 (M_w 6.8); therefore, the hazards they pose are nearly equal to those from other seismic sources for time scales relevant to retrofitting structures. The 2001 Nisqually earthquake caused over billion in losses. While retrofitting limited damages, continued efforts are needed because an earthquake closer to Seattle or larger in magnitude will cause more damage and disruption. The reexamination of historical earthquake seismograms and analysis of modern digital seismograms from recent earthquakes improves strong motion prediction more than stochastic scenarios and better resolves how stresses are released in the subducting plate relative to stresses from external tectonic forces and local dehydration. Reanalysis of the 1949 Olympia, Washington earthquake using digitized seismograms yielded a mechanism that resembles those from previous normal-slip PS intraslab earthquakes. The strike-slip mechanism previously estimated in 1987 contrasted greatly because past PS intraslab earthquakes all have normal-slip mechanisms. We fit the seismograms recorded by global stations to estimate a model for the rupture process of the earthquake with and without model assumptions. Both simple and complex models are consistent in distribution of rupture and total size. The total size is represented by the seismic moment ($M_o = 1.9\times10^{26}$ dyne-cm) or moment magnitude (M_w = 6.78). The depths of PS intraslab earthquakes appear to be ~5-10 km below the inferred top of the subducting Juan de Fuca plate indicating that rupture is within the upper portion of the subducting oceanic plate sometimes termed the “slab-crust”. We identify a different M_o versus asperity area scaling relation indicating intraslab earthquakes have higher asperity stress drops (or energy release) which may explain the higher peak ground accelerations than from other earthquakes with the same size.

Reports published

Ichinose, G. A., H. K. Thio, P. G. Somerville, Rupture process and near source shaking of the 1965 Seattle-Tacoma and 2001 Nisqually intraslab earthquakes, Geophys. Res. Lett., 31, L10604, doi: 10.1029/ GL019668, 2004.